Electron-drift-mobility measurements and exponential conduction-band tails in hydrogenated amorphous silicon-germanium alloys

Qi Wang, Homer Antoniadis,* and E. A. Schiff
Department of Physics, Syracuse University, Syracuse, New York 13244-1130

S. Guha
United Solar Systems Corporation, 1100 West Maple Road, Troy, Michigan 48084
(Received 17 August 1992; revised manuscript received 14 December 1992)

We have measured the temperature dependence of the electron drift mobility using the time-of-flight technique for a series of undoped hydrogenated amorphous silicon-germanium alloys with band gaps spanning the range 1.47–1.72 eV. We also developed techniques for analyzing dispersion effects in such measurements, which permitted us to compare essentially all previous measurements with our own. We draw two main conclusions. First, there is *substantial agreement* between laboratories for the reduction in the electron drift mobility due to Ge alloying. Second, we are able to account for most of the features of the data using the standard multiple-trapping model by invoking *only* variations of an exponential conduction-band-tail width $\mathcal{E}_C^0$; we find a fair linear correlation between this width and the optical band gap $\mathcal{E}_T$. The effects of alloying upon the microscopic mobility and the attempt-to-escape frequency were relatively minor.

I. INTRODUCTION

Photocarrier transport in amorphous semiconductors is perhaps best studied using the time-of-flight method, which measures the transit time t_T for a sheet of photocarriers through a distance L under an electric field E. The resulting data typically exhibit the phenomenon of "dispersion": the transit times are *not* proportional to the distance L for a given field.[1,2] Dispersive transport is obviously more difficult to describe than ordinary, Gaussian transport, where photocarrier transit times are proportional to distance. However, it turns out for several materials that the details of dispersive transport can largely be understood in terms of *multiple trapping*[3–6] of the photocarriers. Transport is attributed only to the "microscopic mobility" of carriers in band states above a transport edge. Carriers trapped in localized states below the edge must wait to be thermally emitted back above it before they again contribute to transport.

In undoped a-Si:H most studies of electron time of flight are broadly consistent with the results expected for an exponential distribution of conduction-band-tail states;[7–11] the exponential width $\mathcal{E}_C^0$ is typically 25 meV. This is a truly remarkable result: the considerable complexity of electron transit-time measurements as a function of specimen thickness and temperature has been condensed into a single parameter.

More recently electron time-of-flight measurements have been conducted in hydrogenated amorphous silicon-germanium alloys (a-$Si_{1-x}Ge_x$:H). These alloys are of considerable technological interest because they have smaller optical band gaps than a-Si:H; some of the history of this material has been reviewed by Stutzmann *et al.*[12] All of the drift-mobility reports have reached the same qualitative conclusion that Ge alloying diminishes the electron drift mobility, primarily due to broadening of the conduction-band tail.[13–20] Despite the basic success of band-tail multiple trapping and the extensive research on electron drift in the a-$Si_{1-x}Ge_x$:H system, a quantitative description of the relationship of electron drift to other materials parameters has not emerged. It is also not possible to directly compare the multiple-trapping-model parameters proposed by different groups, since fitting procedures and certain model refinements vary substantially between groups.

In the present paper we shall attempt to give a comprehensive description of the electron mobility in a-Si:H and a-$Si_{1-x}Ge_x$:H. We report a series of electron-drift-mobility measurements in a-$Si_{1-x}Ge_x$:H over a larger range of optical band gaps than obtained previously. This range was possible due to continuing improvement in the quality of a-$Si_{1-x}Ge_x$:H. We also present techniques which we used to compare electron transit-time measurements in different materials. Using these techniques, we found a remarkably simple pattern to the measurements on all specimens to date.

This result is presented in Fig. 1, where we have plotted our estimates of the temperature-dependent drift mobility $\mu_D \equiv d/2Et_T$ for ten specimens of a-$Si_{1-x}Ge_x$:H. d is the specimen thickness; as will be discussed subsequently, the factor 2 in the above definition reflects the fact that the transit time t_T usually corresponds to an average electron displacement L of half the specimen's thickness $L = d/2$. In this figure we have presented estimates for multiple specimens using a single value of $d/2E = 2 \times 10^{-9}$ cm^2/V; this is a crucial refinement for comparing specimens exhibiting dispersive transport. Four of the specimens were measured in the present work, and the remaining six specimens are from previously published measurements by other groups. The three up-

per curves are unalloyed a-Si:H; the successively steeper curves correspond to a-$Si_{1-x}Ge_x$:H specimens of increasing Ge content x and decreasing band gap.

The simple pattern which we discern in these data is indicated by the straight lines which focus at $\mu_D = 10^3$ cm^2/V s for $1/T = 0$. This simple behavior is an extended prediction of the exponential band-tail, multiple-trapping-model. It has given us a laboratory-independent picture that we have illustrated in Fig. 2 as the density of states suggested by electron time-of-flight measurements on a-$Si_{1-x}Ge_x$:H and by optical measurements. As the band gap $\mathcal{E}_g \equiv \mathcal{E}_C - \mathcal{E}_V$ shrinks, the width of the conduction-band tail $\mathcal{E}_C^0$ grows. We have arbitrarily set the zero of the energy scale at the top of the valence-band tail; photoemission studies indicate that the valence-band tail rises towards the vacuum level with alloying.[21] We have not indicated any changes in the valence-band-tail width with Ge alloying. This is based primarily upon the observation that the "Urbach" parameter estimated from interband optical transmittance studies varies little with alloying.[17,22,23]

The choice we made in Fig. 1 to make all the fitting lines converge at $1/T = 0$ means that we kept the attempt-to-escape frequency ν of band-tail traps constant; we were fairly successful in dealing with all available data by keeping the microscopic mobility (μ_0) constant as well, and allowing variation *only* in $\mathcal{E}_C^0$. This simple, indeed reductionist, procedure is a departure from the more detailed models of previous groups, which have incorporated nonexponential band tails, alloy dependence of additional multiple-trapping parameters, and extensions of multiple trapping to include other transport processes.[11,18,24] Our intention is to assess the value of the simplest reasonable model for transport in a-$Si_{1-x}Ge_x$:H.

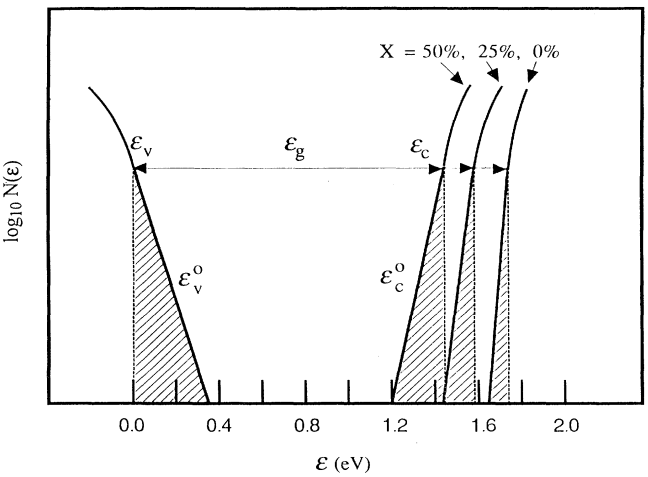

FIG. 2. Schematic density-of-states diagram in a-$Si_{1-x}Ge_x$:H. Three conduction-band edges and tail states, with indicated $x = 0\%$, 25%, and 50% (in at.%), have been drawn in scale referring to valence-band edge. The shadow regions are band-tail states. It has been shown that the conduction-band width increases linearly as the band gap shrinks.

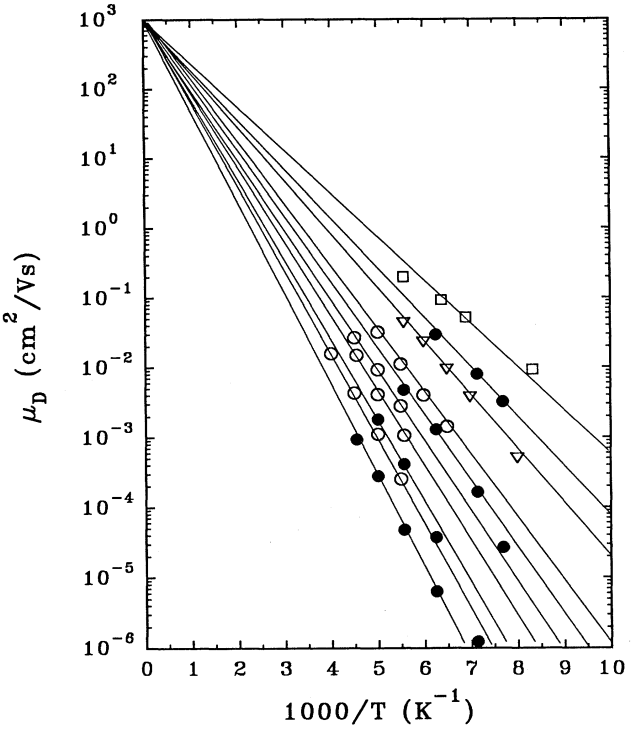

FIG. 1. Average electron drift mobility for ten specimens of a-$Si_{1-x}Ge_x$:H as a function of reciprocal temperature. All points correspond to a ratio $L/E = 2 \times 10^{-9}$ cm^2/V between the electron displacement and the external electric field. References to the sources are given in Fig. 15. The straight lines drawn through the data are fits to the standard exponential band-tail multiple-trapping model. Only one parameter, the conduction-band-tail width $\mathcal{E}_C^0$, was adjusted for each specimen. The trend which we discern is the focus point at $\mu_D = 10^3$ cm^2/V s for $1/T = 0$ converged by the straight lines extended to an unphysical regime for $\mu_D > 1$ cm^2/V s.

As is evident in Fig. 1, the simplest model does account for most of the features of the data. In addition, this simplified approach yielded a useful correlation of the fitting parameter $\mathcal{E}_C^0$ with the band gap $\mathcal{E}_T$ based on Tauc plots. The correlation is presented in Fig. 3. Although there is considerable scatter, the measurements suggest that there is a *linear* relationship between $\mathcal{E}_T$ and $\mathcal{E}_C^0$ in the range shown.

The present paper is organized as follows. In Sec. II we present technical details regarding the specimens and our transport measurements. In Secs. III and IV we present a detailed discussion of the procedures we employ to obtain and analyze data about dispersive transport. We exploit a simple but crucial result: transit times t_T are uniquely defined for a given material by the ratio L/E of the displacement L and the electric field E. This result is a consequence of transport which is linear in electric field, and transcends more specific transport models. We also show that photocharge transient measurements are a convenient alternative to conventional transit-time measurements for determining the L/E vs t_T relationship.

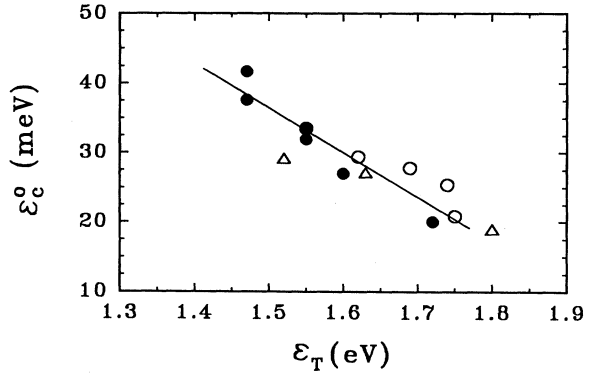

FIG. 3. Summary plot of the correlation between conduction-band-tail width $\mathcal{E}_C^0$ and Tauc gap $\mathcal{E}_T$ in a-$Si_{1-x}Ge_x$:H. Note the roughly linear relationship as guided by the line. Sources for the data are •, ECD/SU, this work; ○, Stuttgart (Refs. 16 and 19); △, Siemens (Ref. 14).

In Sec. V we present our measurements of electron drift in a-$Si_{1-x}Ge_x$:H. We then present summary plots including both the present and previous research on the dependence of μ_D upon temperature, germanium alloy parameter x, and band gap $\mathcal{E}_T$. Finally in Sec. VI we elaborate on the multiple-trapping fitting procedure whose results are summarized in Figs. 1 and 3, and we compare the fitting we have chosen with previous models for band tails and multiple trapping in a-$Si_{1-x}Ge_x$:H and we discuss the possible reasons for broadening of conduction-band tail in a-$Si_{1-x}Ge_x$:H. In the Appendix we define a criterion for the transit time.

II. SPECIMENS AND INSTRUMENTS

Five types of a-$Si_{1-x}Ge_x$:H material of varying alloy parameter x were studied in the present project; the material was deposited at Energy Conversion Devices, Inc. using plasma deposition techniques.[22] For each type of material (denoted A–E in Table I) several specimens were deposited. The optical transmittance and reflectance were measured for films about 1 μm thick deposited onto glass. We estimated a band gap $\mathcal{E}_T$ using a Tauc plot; these are given in Table I. The alloy parameter x was estimated using an Auger technique. The relationship of the alloy parameter x and the band gap $\mathcal{E}_T$ is somewhat different than in earlier reports.[12,22,25,26] We also estimated the Urbach parameter $\mathcal{E}_U$ from photothermal deflection spectroscopy[27] on these specimens. We found little variation between specimens. The results may be summarized by $\mathcal{E}_U = 47 \pm 3$ meV. Other work has noted an increase in $\mathcal{E}_U$ of 20 meV or more for some deposition procedures as x increased from 0.0 to 0.5.[12,17] Apparently improvements in material quality have largely suppressed this effect; we shall return to this topic in Sec. VI C.

The electrical measurements were done on p-i-n diodes. The middle i layer was undoped a-$Si_{1-x}Ge_x$:H. The top p^+ and the bottom n^+ layers were both 20 nm thick. The principal properties of the specimen diodes are presented in Table I. The thinner series (0.32 μm) was used to obtain solar cells parameters [open circuit voltage V_{0C}, "blue" fill factor FF_B ($\lambda < 450$ nm), and the quantum efficiency at 850 nm Q_{850}]. These measurements were done using a commercial (Oriel, Inc.) solar simulator corresponding approximately to global "air mass" (AM) 1.5. A detailed discussion of these parameters has been given elsewhere.[28]

The diodes with thicker i layers were used for transient photocurrent measurements. Transient photocurrents were measured in these diodes using 3-ns illumination pulses from a nitrogen-laser pumped dye laser. Illumination was through the top p^+ layer. We selected laser wavelengths so that the absorption length was less than 10% of the specimen's thickness. We intentionally avoided more strongly absorbed light to avoid back-diffusion and surface recombination problems.

TABLE I. Properties of a-$Si_{1-x}Ge_x$:H (x in at. %) specimens used in this research. The symbols definitions are as follows: d is the thickness of the i layer, $\mathcal{E}_T$ is the optical gap (from Tauc plots), V_{0C} is the open circuit voltage, FF_B is the fill factor at wavelength less than 450 nm Q_{850} is the quantum efficiency at 850 nm (these properties were measured under AM 1.5 condition), $\mathcal{E}_C^0$ is the conduction-band-tail width, $\mu\tau_{e,t}$ is the electron deep-trapping mobility lifetime product, and $\mu\tau_{h,t}$ is the hole deep-trapping mobility lifetime product (these properties were obtained from the transient photocurrent measurements).

Specimen (a-$Si_{1-x}Ge_x$:H)	A ($x = 0$)	B ($x = 10$)	C ($x = 25$)	D ($x = 50$)	E
$\mathcal{E}_T$ (eV)	1.72	1.60	1.55	1.47	1.42
d (μm)	0.32	0.32	0.32	0.32	0.32
V_{0C} (V)	0.94	0.82	0.74	0.68	0.58
FF_B	0.75	0.70	0.62	0.60	0.50
Q_{850}	0.00	0.00	0.05	0.15	0.18
d (μm)	2.65	0.95	1.25	1.00	
$\mathcal{E}_C^0$ (meV)	20	25	32	41	
$\mu\tau_{e,t}$ (cm^2/V)	6.2×10^{-8}	1.6×10^{-8}	9.2×10^{-9}	5.1×10^{-9}	
$\mu\tau_{h,t}$ (cm^2/V)	6.1×10^{-8}		1.4×10^{-9}	5.5×10^{-10}	

The photocurrent transients reported here are the averages of at least twenty pulses; our averaging technique leads to a 10-ns uncertainty in the arrival time of each pulse. The specimen temperatures reported here are believed accurate to ± 1 K. Further details of the electronic instrumentation and the temperature-dependent cryostat have been given elsewhere.[29]

A reverse bias voltage was applied to the diode about 20 μs ahead of the laser flash; the duration of the voltage pulse was about 200 μs. There was no evidence in the displacement current wave forms for dielectric relaxation during the bias pulse. The intensity of the laser was attenuated with neutral density filters until the photocharge was well below the CV charge measured by integrating the displacement current wave form. The repetition rate of the laser was reduced until the transient photocurrent was independent of repetition rate; a 1-Hz rate was usually allowable. These precautions ensure that the external field in the specimen was essentially uniform during the photocurrent transient.

In Table I we have tabulated the conduction-band-tail width $\mathcal{E}_C^0$ and the deep-trapping mobility-lifetime products of electrons and holes $\mu\tau_e$ and $\mu\tau_h$ obtained from the photocurrent measurements. The deep-trapping mobility-lifetime product is related to the displacement (or range) of a photocarrier R when it is captured by a deep level: $R = \mu\tau_{e,t}E$. For a given field, band-tail-dominated drift mobilities can only be studied using displacements L smaller than this range.

The procedure for estimating $\mathcal{E}_C^0$ will be presented shortly. Deep-trapping mobility lifetime products were estimated at room temperature using the photocharge [the integral of the transient photocurrent $i(t)$] for relatively low voltages V. For electron drift we have $Q(t_C) = \mu\tau_{e,t}VQ_0/d^2$, where t_C is a charge collection time, Q_0 is the total photocharge collected at high voltages, and d is the specimen thickness. t_C must be chosen sufficiently long to ensure that deep trapping has occurred. Hole mobility-lifetime products $\mu\tau_{h,t}$ were measured in an essentially similar way, except that illumination was through the bottom n^+ electrode. A fairly detailed discussion of these techniques has been given elsewhere.[30]

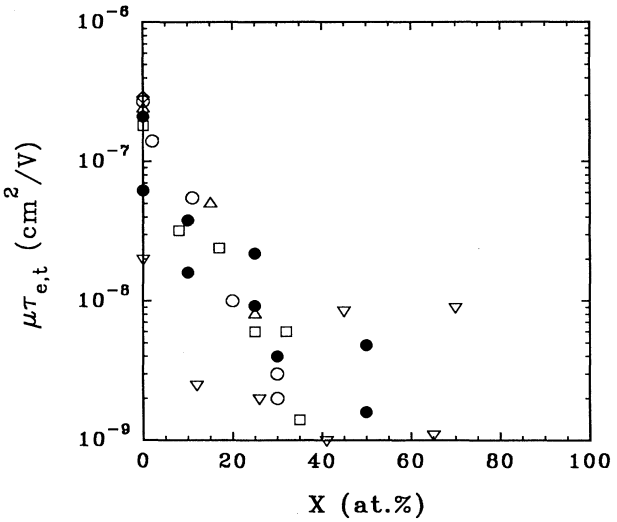

FIG. 4. Correlation of electron deep-trapping mobility lifetime product with of Ge concentration x (in at.%) in a-$Si_{1-x}Ge_x$:H. Sources for the data are •, ECD/SU, this work; ○, Stuttgart (Refs. 16 and 19); ▽, Princeton (Ref. 44); △, Siemens (Ref. 14); □, Harvard (Ref. 45); ◇, Chronar (Ref. 46).

In Fig. 4 we have plotted the published estimates of $\mu\tau_{e,t}$ (at room temperature) as a function of the reported Ge concentration x from numerous sources. The results are not very elegant, although they do indicate the well-known trend that increasing the Ge content in a-$Si_{1-x}Ge_x$:H also increases the deep level density (as gauged by $\mu\tau_{e,t}$). We caution that the procedures used by different groups for estimating $\mu\tau_{e,t}$ vary, as do the procedures for estimating x; the original references should be consulted for more details.

III. TRANSIT TIMES AND DRIFT MOBILITIES IN a-Si:H

In this section we address the general problem of comparing time-of-flight measurements at some specific temperature in different materials. Time of flight measures the transit time t_T required for the mean position of a carrier distribution to move some distance (or *schubweg*) L in a known electric field E; L is usually determined by the thickness of the specimen d, but is not necessarily exactly equal to it. In practice a carrier distribution is generated at some initial time and position by an excitation impulse — a laser pulse in the present work. For ordinary, nondispersive transport, L, E, and t_T are related by the expression

$$L/E = \mu_D t_T. \tag{1}$$

We assume that transport is linear in an electric field.

Experimentally, Eq. (1) can be tested by graphing the relationship of L/E and t_T to test for proportionality; we refer to such graphs as "displacibility plots." In Fig. 5 we have presented some data reported by Marshall, Street, and Thompson[11] correlating transit times for electrons in a-Si:H with $d/2E$, where d is the specimen thickness. As noted earlier, the displacement L of electrons is equal to $d/2$ at the transit time. These data were obtained for a single specimen by varying the electric field. The $d/2E$ vs t_T relationship is quite nonlinear (notice the logarithmic axes). This effect is *not* due to a breakdown of linear transport, but is instead the phenomenon of "dispersion."[2]

Dispersive transport invalidates comparison of specimens using a single value of the drift mobility. At first glance it is unclear how complex a phenomenon dispersion might be. For example, would the same "displacibility" curve be generated if a different specimen thickness had been employed? In comparing transit times for different materials, is it necessary to hold both the specimen thickness and the electric field constant?

It turns out that the displacibility curve in Fig. 5 is a complete representation of transit-time information for

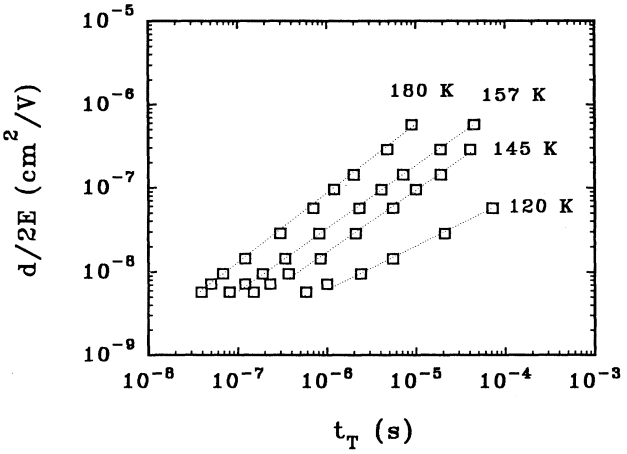

FIG. 5. Displacability plot illustrating the correlation of the transit times t_T and the ratio $d/2E$ of specimen thickness d and electric field E for an undoped a-Si:H specimen deposited at Xerox PARC; results at four temperatures are shown. Dotted lines are guides only. The measurements were reported in Ref. 11.

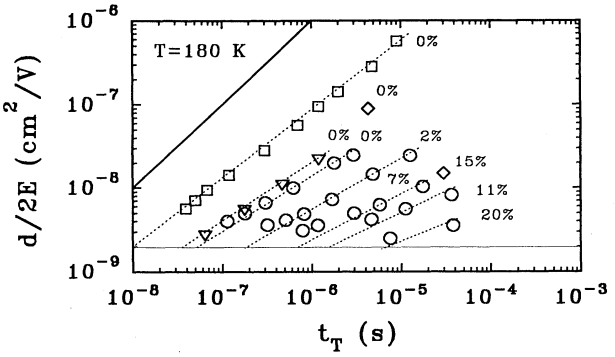

FIG. 6. Displacability plot correlating $d/2E$ and the transit time t_T at 180 K in a-$Si_{1-x}Ge_x$:H. The labels indicate the reported atomic percentage of Ge in each specimen. The specimen origins and literature references are □, PARC (Ref. 11); ▽, CNRS (Ref. 18); ◇, Siemens (Ref. 14); ○, Stuttgart (Ref. 17). The solid line at the top left indicates nondispersive transport with $\mu_D = 1$ cm^2/V s. The horizontal line at $d/2E = 2 \times 10^{-9}$ cm^2/V was used to obtain transit times for computation of the corresponding average drift mobility $\mu_D \equiv d/2Et_T$. The dotted lines shown are multiple-trapping fits assuming $\mu_0 = 1$ cm^2/V s, $\nu = 5 \times 10^{11}$ s^{-1}, and varying the band-tail width $\mathcal{E}_0^C$ as a parameter (see Sec. VI A for details).

linear transport in a given material; the same curve can be generated by varying d or E. The argument is as follows. The most general formulation for linear transport is that the transit time should be determined solely by the ratio L/E. If the electric field E and distance L are both doubled, the transit time should remain unchanged. In mathematical form, we generalize Eq. (1) to read

$$L/E = \zeta(t_T). \tag{2}$$

Physically, Eq. (2) states that the distance traveled by the mean position of a photocarrier distribution in a given time is proportional to the electric field. The function $\zeta(t)$, which we term the *displacibility function*, has the dimensions of a mobility-lifetime product (cm^2/V).

Although these ideas may seem straightforward, they yield several useful insights. First, although the data reported in Fig. 5 were generated by varying the electric field, they could in principle have been obtained by varying the specimen thickness and leaving the electric field constant. Second, it is conventional to report drift mobilities $\mu_D = L/Et_T$ even in dispersive materials. Such drift mobilities depend only on the ratio L/E. In preparing Fig. 1, which presented the temperature dependence of μ_D for ten specimens of a-$Si_{1-x}Ge_x$:H, we were careful to estimate μ_D in all specimens for a single value of L/E.

Finally, a complete presentation of transit-time information in different materials exhibiting dispersion requires that displacibility curves be compared instead of single values of the drift mobility. Although it is not commonly practiced, this procedure proved to be remarkably informative. In Fig. 6 we have graphed the results of several published transit-time studies on a-$Si_{1-x}Ge_x$:H at 180 K in the displacibility format. Note the double logarithmic axes. The graph shows very clearly the variation in electron transport properties for a wide range of amorphous-silicon-based materials. The lower curves, corresponding to slower electron transport, are also more sublinear. We shall interpret this effect in Sec. VI as a second consequence of broadening of the conduction-band tail; the first consequence was the increasing activation energy exhibited by the μ_D vs $1/T$ data presented as Fig. 1.

IV. TECHNIQUES FOR TRANSIT-TIME MEASUREMENTS

The classic time-of-flight technique is practiced by measuring transit times for varying electric fields E in a specimen of some specified thickness. In this section we present raw photocurrent and photocharge data for one specimen of a-Si:H to represent "typical" measurements and to illustrate procedures for obtaining transit times and for making displacibility curves (cf. Figs. 5 and 6). We also show our procedure for verifying that electron transport was linear in electric field. We developed one refinement of the time-of-flight procedure which permits us to obtain displacibility curves over larger ranges of transit times and with much higher resolution than the standard procedures; this refinement will also be described here.

A. Photocurrent and photocharge measurements in a-Si:H

Figure 7 shows the transient photocurrent measurements $i(t, V)$ for varying external voltage V at 130 K. Larger voltages could not be used because of diode breakdown. For voltages less than 1 V the internal field in the

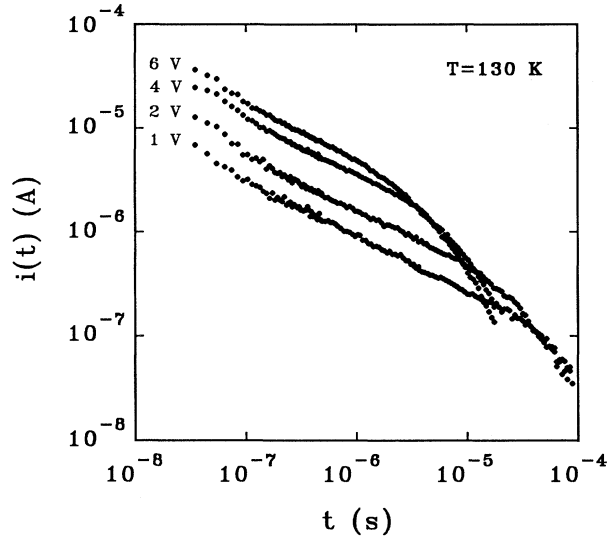

FIG. 7. Transient photocurrents measured in an annealed a-Si:H p-i-n diode prepared at Energy Conversion Devices, Inc. (ECD) (specimen A from Table I). The transients were measured at 130 K using the indicated external bias voltages.

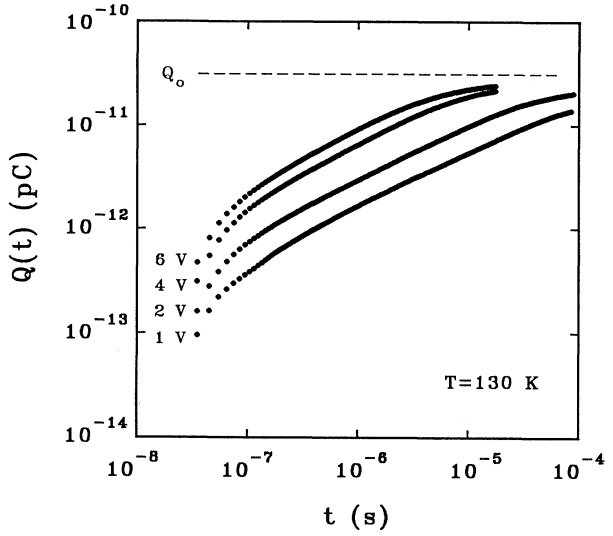

FIG. 8. Transient photocharges obtained by integrating the photocurrent transients in Fig. 7. The photocharge transients for all four voltages approach the total photocharge Q_0 at longer times.

diode is important, and we have chosen not to present the low-voltage data.

The measurements are typical of photocurrent transients exhibiting transit times and dispersions. At low voltages there is little evidence for photocarrier sweepout; the current declines as a power law, which is the signature of dispersive transport. The cutoff in the photocurrent for longer times at higher voltages is due to the transit of photocarriers across the specimen; as expected for time of flight, the transit time occurs earlier at higher voltages. Finally, prior to the transit time the current increases essentially proportional to the bias voltage, which is the signature of linear transport.[29]

In Fig. 8, we show the transient photocharge $Q(t,V)$ for varying external voltage V; $Q(t)$ was computed by numerical integration of the transient photocurrent data of Fig. 7. Most of the features are anticipated from the photocurrent data; note that none of the $Q(t)$ curves crosses the line labeled Q_0, which is our estimate of the total mobile photocharge generated near the top surface of the specimen by the laser impulse. For $t < 100$ ns the measurements are affected by the "rise time" of the system, which in this case was largely determined by a series resistance in the connection to the specimen.

Figure 9 shows the temperature dependence of the transient photocharge $Q(t,T)$ at 4 V, with the same fiduciary line Q_0. The behavior in Figs. 7–9 is consistent with a unity quantum efficiency η. In general, $Q_0 = e\eta N_0$, where e is the electronic charge, η is the photogeneration quantum efficient, and N_0 is the number of photons absorbed near the surface of the specimen. The fact that the photocharge reaches the same plateau at different external voltages and at different temperatures indicates that the photogeneration quantum efficiency η is independent of the voltage and the temperature. Comparison of optical estimates of the number of photons absorbed with measured values of Q_0 constrain η to be quite close to unity.[30–32]

B. Transit-time methods

We now turn to methods for determining the transit time from photocurrent and photocharge measurements. The *method of normalized photocurrents* is illustrated in Fig. 10, where we have replotted the data of Fig. 7 in normalized form $i(t)d^2/Q_0V$; V is the bias voltage, Q_0 is the total mobile photocharge, and d is the specimen thickness. We emphasize the following feature of Fig.

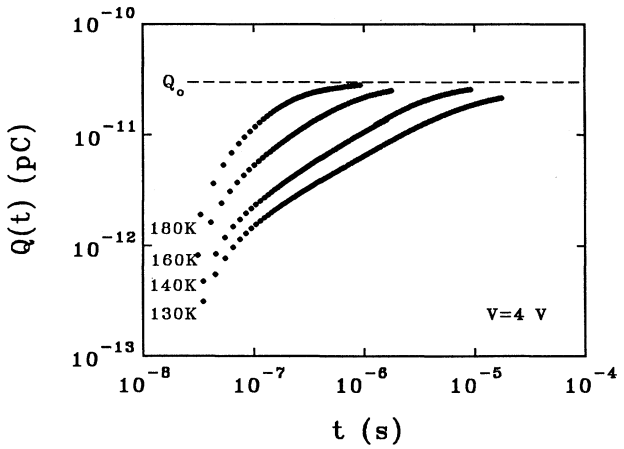

FIG. 9. Photocharge transients measured at 4 V bias (specimen A from Table I) for four specimen temperatures. The photocharge saturates near the same level Q_0 for all temperatures; this value for Q_0 was also illustrated in Fig. 8.

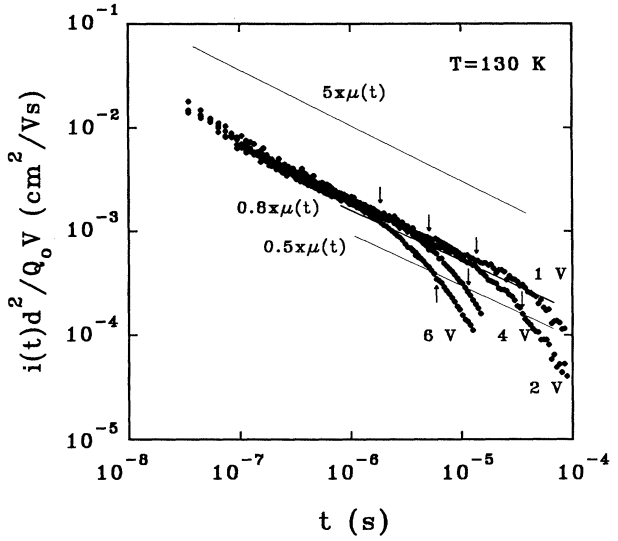

FIG. 10. Normalized transient photocurrents $i(t)d^2/Q_0V$ based on Fig. 7. The congruence of transient photocurrents at early times indicates that transport is linear in the electric field and establishes an *envelope curve* $\mu(t)$. Our estimate of $\mu(t)$ is shown displaced to the top of the figure. Individual transients drop below $\mu(t)$ due to carrier sweepout. Fiduciary lines at $0.8 \times \mu(t)$ and $0.5 \times \mu(t)$ are drawn to illustrate two methods of estimating transit times; the arrows show the resulting transit time estimates.

10. Each curve has two distinct regions: a pretransit domain, with a fairly shallow power-law decay, and the post-transit region, with a fairly steep decay. Note that the pretransit sections of the curves overlap. This congruence is expected if transport is linear, since prior to transit we expect that photocurrents should be "Ohmic." We attribute the slight imperfection of this overlap primarily to the effects of unknown internal fields.

The common pretransit envelope curve [the $\mu(t)$ curve shown near the top of the figure] is the basis for the method of normalized photocurrents. Marshall, Street, and Thompson[11] have defined the transit time t_T as the crossing point of the envelope curve and the curve $0.8 \times \mu(t)$; we shall refer to this procedure as the "80% method." Nebel and co-workers[16,19] used the crossing of the normalized photocurrent and the curve $0.5 \times \mu(t)$; this obviously gives somewhat larger values for a transit time.

As is evident from the above, transit-time estimates based upon the transient photocurrent transient tend to be slightly arbitrary. Procedures based upon the photocharge transients are somewhat easier to defend, although we shall see that they give similar results. For example, a third technique which we have found useful is to estimate the time at which half the ultimate photocharge is collected (see the Appendix). This "half-charge" technique is based on the fact that, prior to the onset of carrier transit, the photocharge $Q(t)$ is proportional to the distance moved by the mean position of the photocarrier distribution.

In particular, the electrostatic energy dissipated by a charge Q_0 of photocarriers drifting in a uniform electric field E is $Q_0x(t)E$. We assume that internal electric fields are negligible. This energy dissipation can be equated to the energy furnished by the electrical bias voltage $Q(t)V$; $Q(t)$ is the charge that has passed through the external bias circuit in order to maintain the potential V across the specimen. After some algebra we obtain

$$x(t) = d\frac{Q(t)}{Q_0}. \tag{3}$$

We have used $E = V/d$. Thus when $Q(t)$ reaches $Q_0/2$, the mean position of the photocarrier distribution has moved about $d/2$. This is the origin of our claim that the displacement L of the photocarrier distribution at the transit time t_T is *half* the specimen thickness.

Equation (3) suggests a still better approach to determining the time required for the mean of a photocarrier distribution to drift some specified distance L. Recall that the displacibility $\zeta(t)$ is the function describing the dependence of the ratio L/E to a transit time t_T. We now generalize the definition of $\zeta(t)$ to be the ratio $x(t)/E$, thus obtaining

$$\zeta(t) = Q(t)\frac{d^2}{Q_0V} \quad (t \ll t_T). \tag{4}$$

We shall call this fourth method the *normalized photocharge* technique. We compare the four procedures using experimental data in the next subsection.

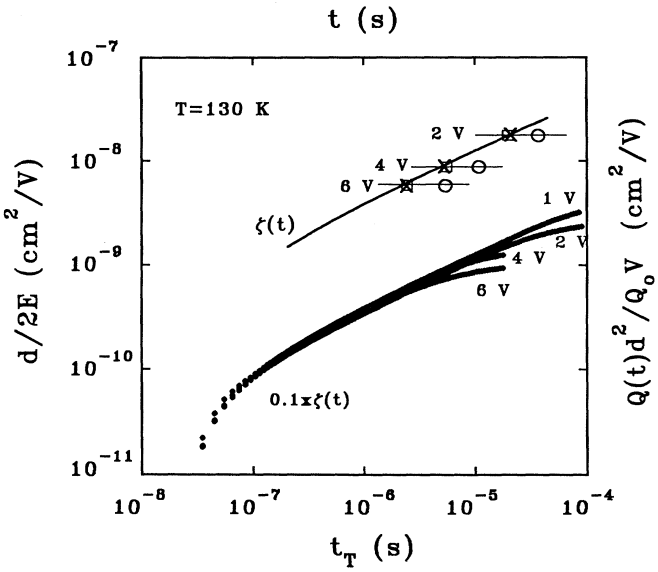

FIG. 11. The lower portion of the figure illustrates the time integral $Q(t)d^2/Q_0V$ of the normalized photocurrent transients from Fig. 10. These normalized photocharge transients determine an envelope or *displacibility* function $\zeta(t)$ illustrated in the upper portion of the figure. The symbols are estimates of the displacibility function obtained by correlating $d/2E$ with transit times estimated with the 80% criterion (□), the 50% criterion (○), and the half-charge criterion (×). Note the satisfactory agreement of the two different procedures for evaluating $\zeta(t)$.

C. Transit-time measurements

The symbols in the upper portion of Fig. 11 are transit-time estimates plotted against the ratio $d/2E$, where d is the specimen thickness. The open squares were obtained using the 80% technique for determining the transit time from the photocurrent data of Fig. 10; the open circles indicate transit times determined using the 50% criterion and Fig. 10. We also indicate with crosses the transit time determined from half collection of the photocharge (cf. Fig. 8). The 80% method and the half-charge method agree well. The 50% method yields a larger value of the transit time; we have found no entirely satisfactory procedure for estimating the displacement associated with this procedure or for converting between it and others.

In the lower portion of the figure we have graphed the normalized transient photocharge measurements $Q(t)\frac{d^2}{Q_0V}$; the data are displaced from the transit time data for clarity. Note the common ($t \ll t_T$) envelope of these data. For a given voltage the normalized photocharge is reasonably congruent with the envelope until it approaches d^2/V, which is the largest value $Q(t)\frac{d^2}{Q_0V}$ can obtain. Empirically a given transient $Q(t)\frac{d^2}{Q_0V}$ is congruent with the envelope until the time it reaches about $d^2/2V$, which is the half-charge estimate of a transit time.

The solid line passing through the crosses and the squares in the upper portion of the figure is the envelope of the normalized transient photocharge measurements; we have not shown the envelope before 300 ns because the specimen series resistance affected this regime. It is clear that this method is consistent with direct transit-time measurements using either the half-charge or 80% procedure. There are two advantages of the normalized photocharge technique over direct transit-time measurements. First, it is more efficient. A handful of transients were sufficient to obtain a continuous curve. Second, we obtained the displacibility for shorter transit times than were accessible directly by increasing the bias voltage.

V. ELECTRON DRIFT MOBILITIES IN a-$Si_{1-x}Ge_x$:H

A. Measurements on ECD specimens

In Fig. 12 we have presented $\zeta(t)$ curves (our estimate of the relationship of L/E to the transit time t_T) measured on four specimens of a-$Si_{1-x}Ge_x$:H at four temperatures; these curves were obtained using photocharge transients as described in the preceding section. The early time cutoffs in these data were chosen to minimize the effects of the electrical rise time; for most specimens the rise times were determined by series resistance of the electrodes. The later time cutoffs were indirectly dictated by the necessity of using voltages large enough to make internal field effects negligible; for these voltages carrier sweepout determined the longest times at which $\zeta(t)$ could be plotted.

Displacability graphs such as Fig. 12 are not a conventional way of representing electron-drift-mobility measurements. In Fig. 13 we have presented a more conventional representation of such measurements; in particular we have graphed $\mu_D \equiv L/Et_T$ as a function of reciprocal temperature $1/T$ for several values of the electric field E in a-Si:H. To calculate μ_D we determine a transit time for some particular value of L/E using the displacability curves of Fig. 12. Figure 13 is very similar to previous work on a-Si:H; we shall make a more quantitative comparison subsequently.

The $\zeta(t)$ curves of Fig. 12 can be approximately described using power laws $\zeta(t) \propto t^{\alpha}$, where α is a "dispersion" parameter.[6,10] We estimated α for each specimen and temperature by measuring the slope of each line. In

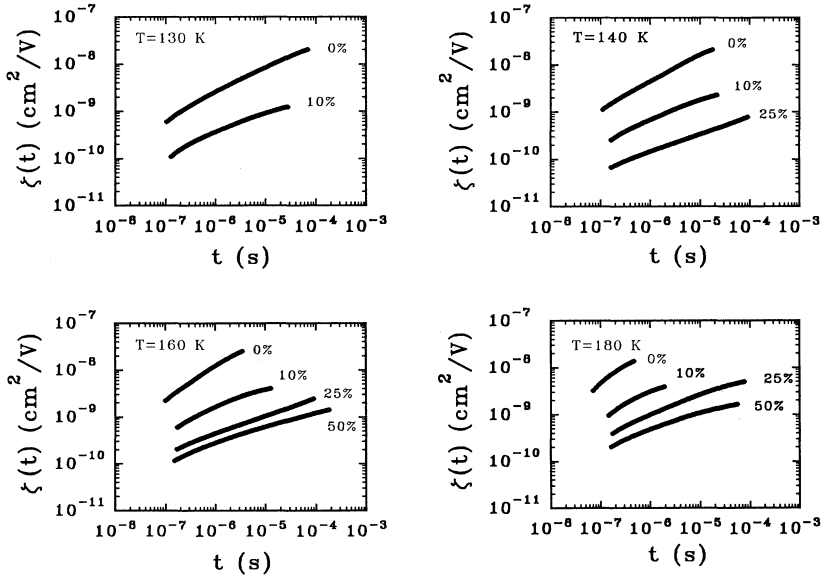

FIG. 12. Displacibility functions $\zeta(t)$ (relation of L/E and transit time) for a-$Si_{1-x}Ge_x$:H specimens with indicated germanium atomic percentages. The four panels illustrate measurements at four temperatures. The displacibilities were estimated using transient photocharge techniques; specimen details are given in Table I.

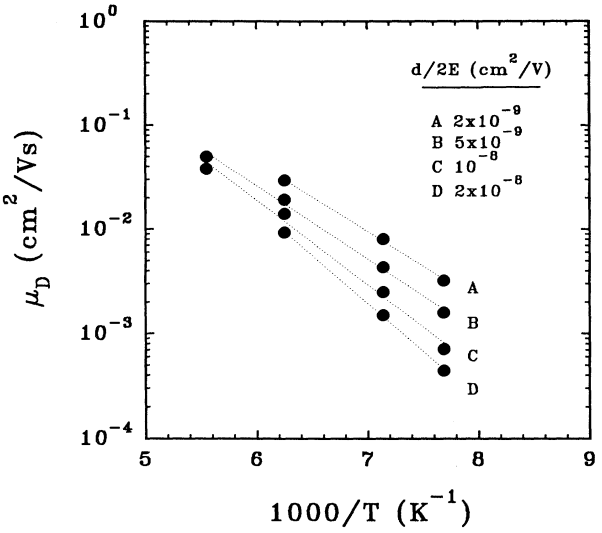

FIG. 13. Average electron drift mobility μ_D as a function of reciprocal temperature in the annealed a-Si:H specimen (specimen A from Table I). Results are shown for four values of $d/2E$; the different curves result from dispersion effects.

Fig. 14 we present the temperature dependence of the dispersion parameter estimates for each specimen. We have also illustrated a straight line through the measurements for each specimen representing the relation $\alpha(T) = T/T_C$; this relationship is expected if the drift mobility is due to multiple trapping in an exponential band tail of width $\mathcal{E}_C^0 = k_B T_C$. T_C generally increases with increasing alloy parameter x. We shall discuss this model extensively in Sec. VI.

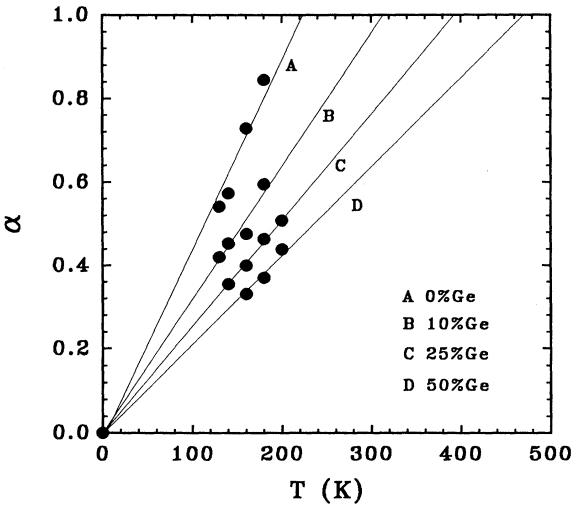

FIG. 14. Dispersion parameter α as a function of measurement temperature for four a-$Si_{1-x}Ge_x$:H (x in at. %) specimens described in Table I. The straight lines indicate the proportionality of α and T anticipated from multiple trapping in an exponential band tail; the characteristic temperature of the band tail T_C can be estimated from the slopes of the fitting lines.

B. Summary of previous measurements

In Fig. 6 we have presented previous electron time-of-flight measurements in a-$Si_{1-x}aGe_x$:H at 180 K. In particular we plotted the correlations of the reported transit times and the corresponding values of $d/2E$, where d is the specimen thickness and E is the electric field across the specimen. In order to prepare this graph we needed to recalculate transit times from reported μ_D results. For the Siemens specimens studied by Karg, Krühler, and Möller[14] only a single point was reported for each temperature. The qualitative features of these data are similar to those for the energy conversion devices (ECD) specimens we measured: Ge alloying diminished the drift mobility and additionally decreased the dispersion parameter.

In order to compare the temperature-dependent electron drift of specimens with varying alloy parameter x we considered the drift mobility $\mu_D \equiv L/Et_T$ corresponding to a fairly small value of $d/2E = 2 \times 10^{-9}$ cm^2/V. For most specimens this required us to extrapolate the measured correlation between the transit times t_T and $d/2E$. We also computed μ_D for our own measurements on ECD specimens presented in the preceding section; these measurements generally did not require any extrapolation procedure.

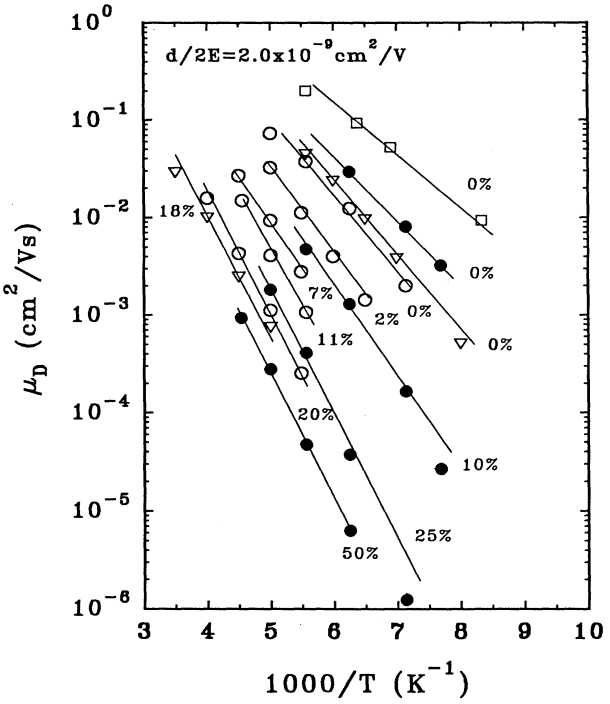

FIG. 15. Summary plot of average electron drift mobility μ_D as a function of reciprocal temperature $1/T$ for twelve specimens of a-$Si_{1-x}Ge_x$:H; these results were also illustrated in Fig. 1. All estimates correspond to a ratio $L/E = 2 \times 10^{-9}$ cm^2/V of carrier displacement to electric field. Work from different laboratories is indicated by different symbols; curves are labeled by the reported Ge atomic percentages. References to the work are •, ECD/SU, this work; □, PARC (Ref. 11); ▽, CNRS (Ref. 18); ○, Stuttgart (Ref. 17).

The resulting family of μ_D vs $1000/T$ curves is presented with semilogarithmic scales in Fig. 15. The behavior of this family seems remarkably systematic. Specimens with larger values of μ_D at some given temperature exhibit the shallowest slope. Figure 1 of the Introduction presented these data along with lines representing multiple trapping in an exponential band tail; we shall address these fits in Sec. VI. These systematic results seem particularly encouraging because they suggest that the work of many laboratories on a-$Si_{1-x}Ge_x$:H should lead to a single unified view for electron transport in this materials system.

In Fig. 16 we have correlated the value of μ_D from Fig. 15 at two temperatures with the alloy parameter x reported by each group. With the exception of the Centre National de la Recherche Scientifique (CNRS) point at 0.18 all values of x are based upon electron microprobe analysis. The CNRS x was based on the proportion of Si and Ge in the deposition gases, which is not generally equivalent to x in the specimen. There is considerable scatter in these data, although the broad trend that increasing x diminishes μ_D is plainly discernible.

The idea that the alloy parameter x should determine μ_D is oversimplified, since even for unalloyed a-Si:H modification of other deposition parameters affects drift mobility measurements and other specimen parameters such as the band gap. For $x = 0$ different groups reported μ_D at 200 K which vary by a factor of about 5. In Fig. 17 we have correlated the value of μ_D from Fig. 15 at two temperatures with reported values of the band gap $\mathcal{E}_T$ determined using the Tauc procedure. In principle this procedure might yield less variance than graphing μ_D vs x, but this is not evident in the figure.

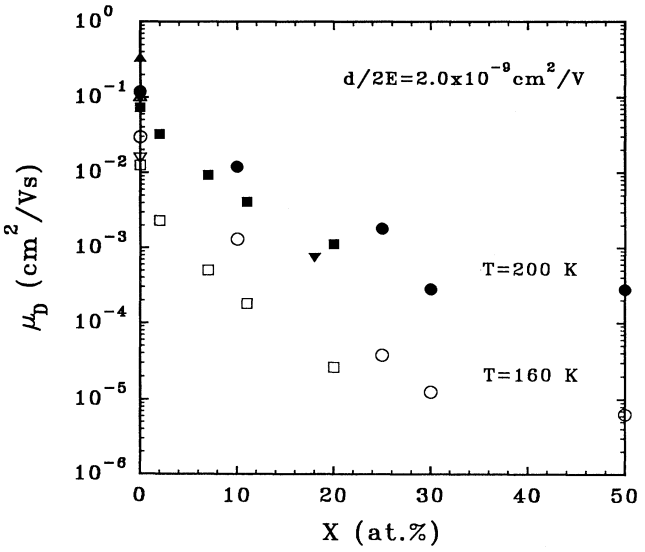

FIG. 16. Correlation of the average electron drift mobility μ_D with the reported concentration of Ge in a-$Si_{1-x}Ge_x$:H. Drift mobilities μ_D correspond to $d/2E = 2 \times 10^{-9}$ cm^2/V; results are shown for two measurement temperatures. Hollow symbols are at 160 K and solid ones are at 200 K. References are ○, ECD/SU, this work; △, PARC (Ref. 11); ▽, CNRS (Ref. 18); □, Stuttgart (Ref. 17).

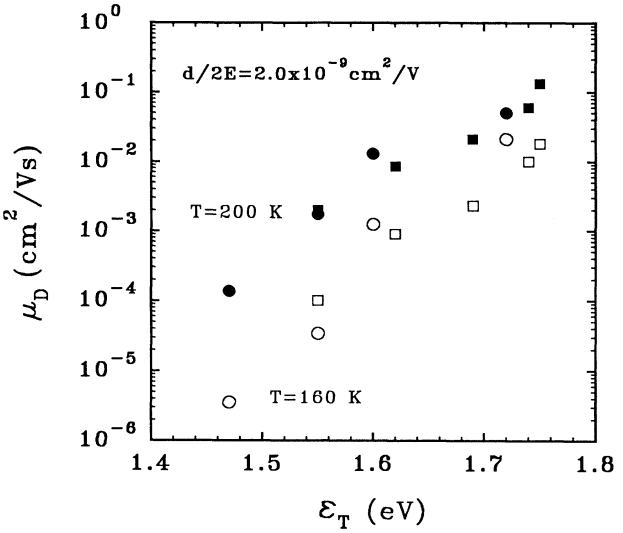

FIG. 17. Correlation of the average electron drift mobility μ_D with the reported optical gap $\mathcal{E}_T$ in a-$Si_{1-x}Ge_x$:H. Drift mobilities μ_D correspond to $d/2E = 2 \times 10^{-9}$ cm^2/V; results are shown for two measurement temperatures. Hollow symbols are at 160 K and solid ones are at 200 K. References are □, Stuttgart (Ref. 17); ○, ECD/SU, this work.

VI. ELECTRON DRIFT AND EXPONENTIAL BAND TAILS IN a-$Si_{1-x}Ge_x$:H

A. Fittings

In this section we discuss fitting the drift mobility data presented in Sec. IV using the model of multiple trapping in an exponential band tail. This model has been extensively described elsewhere.[6,10] The multiple-trapping model[3,4] divides electronic states into transport states (in which electrons are mobile) and traps, which simply immobilize electrons until they can be thermally emitted over some energetic barrier to reenter the transport states. We used the following relationship obtained from the exponential band-tail model:

$$\zeta(t) \equiv L/E = (\mu_0/\nu)(\nu t)^{T/T_C} \quad (T \leq T_C). \tag{5}$$

As before L is the carrier displacement at a time t after photogeneration in an electric field E. T_C is a temperature determined by the energy parameter $\mathcal{E}_C^0 = k_B T_C$ of the exponential band tail. ν is the attempt-to-escape frequency characterizing thermal emission of an electron from a trap (back into the transport states). If the transport edge lies in the exponential band tail, then μ_0 may be interpreted as the mobility of a mobile (untrapped) electron. This equation for $\zeta(t)$ is based on Eq. (6.7) of the review article of Tiedje;[10] a useful alternate perspective was presented by Orenstein, Kastner, and Vaninov.[6] We have neglected a term $1 - (T/T_C)$ multiplying the right-hand side of Eq. (5) above. Tiedje's expression is an approximation in any case; for the special case $T/T_C = 1/2$ the neglected term can be computed exactly,

leading to the value $\pi/4$. We saw no reason to complicate the form of Eq. (5) by inclusion of an approximate term of order unity.

The simple exponential, multiple-trapping model has three free parameters: $\mathcal{E}_C^0$, μ_0, and ν. In principle one might attempt to fit measurements for each specimen using these three parameters; this approach has been used in most previous work on a-$Si_{1-x}Ge_x$:H. In studying the summary plot in Fig. 1, it occurred to us that an even simpler approach might largely account for the measurements. In particular we chose the values $\mu_0 = 1.0$ cm^2/V s and $\nu = 5 \times 10^{11}$ s^{-1}; these were kept the same for all specimens.

Thus only the band-tail width $\mathcal{E}_C^0$ remains as a free parameter; we chose this parameter based on a best fit to displacibility curves. In Fig. 18 we illustrate the resulting fittings for four specimens of a-$Si_{1-x}Ge_x$:H. Our fitting procedure requires that the straight lines representing power-law fits for each specimen all meet at the focus point denoted by the circle. This fitting scheme describes the two upper sets of measurements (PARC and CNRS) very well. For the 7% specimen (Stuttgart) the data can be fitted better using a larger parameter μ_0 and a larger value of $\mathcal{E}_C^0$; the earliest transit time point deviates about 40% from the fitting line. The 25% specimen (ECD/SU) was measured as part of the present work; we cut measurements at early times because of series resistance effects, and we cut measurements at longer times because these were affected by deep trapping. Any true deviation from the fitting lines is probably masked by these effects. The reader may wish to examine the additional fittings to this model shown in Fig. 6.

Since we have used the 180-K data to determine the parameter $\mathcal{E}_C^0$, there are no remaining free parameters.

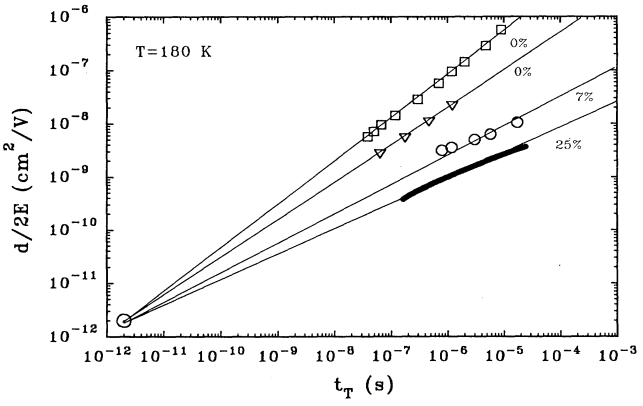

FIG. 18. Displacibility plots $\zeta(t)$ (relationship of L/E and transit time) at 180 K for four specimens of a-$Si_{1-x}Ge_x$:H with indicated Ge atomic concentration. The lines drawn through the data are fits to the exponential band-tail multiple-trapping model allowing variation only in the band-tail width $\mathcal{E}_C^0$; the other multiple-trapping parameters were $\mu_0 = 1.0$ cm^2/V s and $\nu = 5 \times 10^{11}$ s^{-1} for all specimens. References are □, PARC (Ref. 11); ▽, CNRS (Ref. 18); ○, Stuttgart (Ref. 17); •, ECD/SU, this work.

A reasonably stringent test of the fitting approach we are using is the temperature dependence of the drift mobility μ_D. In the exponential band-tail multiple-trapping model $\mu_D \equiv L/Et_T$ is calculated by setting $\zeta(t_T) = d/2E$ in Eq. (2). We obtain, after some algebra,

$$\mu_D = \mu_0(L\nu/\mu_0 E)(L\nu/\mu_0 E)^{-T_C/T} \quad (T \le T_C). \tag{6}$$

In Fig. 1 we presented a comparison of these predictions with the temperature-dependent data of Fig. 15. Note that we have extended the exponential behavior of Eq. (6) to temperatures $T > T_C$, which is an unphysical regime. Of course the maximum mobility measurable within the model is μ_0. The fittings in Fig. 1 seem altogether satisfactory. We conclude that the model of electron transport in a-$Si_{1-x}Ge_x$:H invoking a variable conduction-band-tail width $\mathcal{E}_C^0$ and material-independent parameters μ_0 and ν describes most features of the measured electron drift mobility in a-$Si_{1-x}Ge_x$:H.

Finally, we explored the relationship of the parameter $\mathcal{E}_C^0$ to other materials properties. We discovered that $\mathcal{E}_C^0$ depended approximately linearly upon the optical bandgap measured using the Tauc method; the correlation of $\mathcal{E}_C^0$ and $\mathcal{E}_T$ is presented in Fig. 3.

B. Alternative fittings

In this section we compare the present fitting procedure to some earlier work on a-$Si_{1-x}Ge_x$:H alloys. We commence by discussing the range of the exponential band tail to which the present fittings apply. Time-of-flight measurements roughly probe tail state energies starting at $k_BT\ln(\nu t_M)$ below the transport edge,[10] where t_M is the earliest transit time estimated. Using $t_M = 100$ ns and $T = 120$ K, we estimate a shallowest energy of about 0.11 eV. For time-of-flight measurements the deepest energy states accessed are determined mainly by deep-trapping effects. Assuming that exponential band tails describe drift mobility until deep trapping, we find that the deepest energy accessed is $\mathcal{E}_C^0 \ln(\mu\tau_{e,t}\nu/\mu_0)$. This result was obtained from Eq. (5) and $\mathcal{E} = k_BT\ln(\nu t)$; note that the result is independent of temperature. We find that the deepest energy probed by the present experiments was about 210 meV for a-Si:H and 320 meV for a-$Si_{1-x}Ge_x$:H (x=0.5). Time-of-flight measurements appear to be adequately explained by a simple exponential conduction-band tail within this energy domain.

If the model of material-independent values for $\mu_0 = 1$ cm^2/V s and $\nu = 5 \times 10^{11}$ s^{-1} is accepted, we believe that these parameters are established for the present fittings to within about a factor 2. The value for ν is largely determined by the focus point in Fig. 1; the value for μ_0 is determined by the focus point of Fig. 18. A more stringent claim of constancy has been made recently by Fauchet *et al.*[33] These authors propose that μ_0 is constant to within about 20% in a-$Si_{1-x}Ge_x$:H based on the optical properties of a dense, photocarrier plasma generated using femtosecond laser pulses.

We comment briefly on the significance of the fitting parameter μ_0. The equality of the fitting parameter μ_0

to any "microscopic" mobility requires that the simple exponential form for the band tail continue to the transport edge. If this is untrue, a fitting of μ_0 will depend upon the range of band-tail energies probed in a given experiment. In fact $\mu_0 = 1$ cm^2/V s is clearly too small to account for high-temperature measurements, where electron drift mobilities exceed 1.0 cm^2/V s.[34,17,35] Within multiple trapping, actual drift mobility measurements are a lower bound to the microscopic mobility.

Possible deviations from a simple exponential band tail have in fact been examined by several previous authors.[36,11,16,18] For example, Marshall, Street, and Thompson[11] suggested a linear form for the density of states. In Fig. 1 the upper curve represents these data; it is clear that the temperature dependence of μ_D is not completely explained by the simple exponential fitting for this specimen. Nebel, Weller, and Bauer[16] and Longeaud and Vanderhagen[18] allowed for nonexponential forms in their fittings on individual specimens. However, these fittings do not generally reveal significant deviations from exponential behavior within the limited range of energies accessed by time-of-flight methods. For deeper states probed by the post-transit technique there is fairly strong evidence for deviations from the single-exponential model.

There is also wide variation in previously reported values for μ_0 and ν.[14,17–19,24] μ_0 ranges from 10 to 30 cm^2/V s. ν varies from 8×10^{11} to 5×10^{12} s^{-1} in recent work, with a value as large as 5×10^{14} s^{-1} suggested in the earlier work of Karg, Krühler, and Möller.[14]

Our point of view is the following. In considering data on a single specimen, it is possible to improve fits noticeably by allowing more variability in fitting parameters than we have used. However, when the ensemble of measurements on the a-Si$_{1-x}$Ge$_x$:H system is examined, overall patterns emerge which encourage us to accept somewhat poorer fits to particular specimens in favor of accounting for most measurements with a simpler model.

C. Discussion

The broader conclusion that the conduction-band-tail width increases as the optical gap decreases was reached in previous drift-mobility research, as indeed is necessitated by measurements such as those presented in Fig. 1. We have reanalyzed the previous measurements to obtain the results for $\mathcal{E}_C^0$ summarized in Fig. 3, but the new fittings do not differ greatly from those proposed in the original references. As noted earlier, we decided not to consider the possibility of deviations from the exponential form of the density of states; improved fits can in principle be obtained by allowing for such deviations.[18,19]

Ultraviolet photoemission spectroscopy using the total photoelectron yield technique has also been applied recently to estimating the conduction-band-tail width by Aljishi *et al.*[37] These authors reported that both Ge alloying and also phosphorus doping increased $\mathcal{E}_C^0$. Perhaps more importantly, these authors reported a strong temperature dependence of $\mathcal{E}_C^0$. No comparable temperature dependence has been proposed based on drift-mobility research, and indeed a strongly temperature-dependent value for $\mathcal{E}_C^0$ is incompatible with the linear dependence of the dispersion parameter α upon temperature found both in the present work (Fig. 14) and in earlier work.

There is probably no significant contradiction between the photoyield and the drift-mobility research. Photoyield measurements of the conduction-band tail are conducted at fairly large temperatures ($T > 300$ K) in order to thermally populate band-tail states with electrons. Drift-mobility measurements are mainly sensitive to the conduction-band-tail width at lower temperatures. Aljishi *et al.* proposed that the temperature dependence of $\mathcal{E}_C^0$ is only observable above an equilibration temperature T^*, where it reflects dynamic thermal broadening. Below T^* either the thermal broadening is "quenched in," leaving a static disorder observed as the conduction-band-tail width $\mathcal{E}_C^0$, or alternatively the thermal broadening becomes negligible compared to some fixed, static broadening mechanism.

We now turn to the correlation of $\mathcal{E}_C^0$ and $\mathcal{E}_T$ in Fig. 3. $\mathcal{E}_C^0$ is usually assumed to reflect some type of structural disorder in a-Si$_{1-x}$Ge$_x$:H, although a conclusive theory for such an effect does not yet exist. The simplest disorder mechanism to envision is disorder due to substitution of Ge for Si in a fixed network. There is evidence for a change in the microstructure of germanium alloyed films which may be more important.[25,38] If this alloying disorder underlies the conduction-band-tail broadening, then one would predict that for a-Ge:H without silicon the conduction-band-tail width $\mathcal{E}_C^0$ might be narrower than the larger values presented in Fig. 3. Quite recently electron drift mobilities have been measured in a-Ge:H with about a 1.25-eV optical band gap, but the measurements are apparently not consistent with multiple trapping in exponential band tails.[20]

It seems most curious that the conduction-band tail can respond to such disorder effects so strongly, when the Urbach parameter from optical measurements (and attributed to the valence-band-tail width) varies very little with alloying. We presume that this effect reflects differing sensitivities of the two band tails to the length scale of disorder. Valence band tails are perhaps more sensitive to short-range disorder, and conduction-band tails to longer-range effects.

Although alloying obviously affects both the band gap $\mathcal{E}_T$ and conduction-band-tail width $\mathcal{E}_C^0$ in a-Si$_{1-x}$Ge$_x$:H, it is certainly not the only important mechanism for changing these properties. a-Si:H prepared without Ge incorporation varies significantly in both its band-gap and band-tail widths. For example, the band-tail width for the a-Si:H specimen of Marshall, Street, and Thompson[11] is substantially narrower than that reported in other a-Si:H materials; regrettably, the band gap of this material was not reported, but based on the correlation established in Fig. 3 we would speculate that the band gap would be larger than for the a-Si:H specimens illustrated.

The simplest conceivable model for the variability of the band gap and conduction-band tail in the a-Si$_{1-x}$Ge$_x$:H system would be to link both properties to a single underlying "disorder" representing both alloying

and other mechanisms. Long-range potential fluctuations are one possible mechanism,[39–42] which has been addressed by several investigators. In this view germanium would act to diminish the band gap of a-$Si_{1-x}Ge_x$:H alloys by broadening the band tails,[23] as opposed to rigidly shifting the entire band.

These ideas concerning the correlation of band-tail widths and optical gaps are very similar to those proposed about ten years ago by Cody *et al.*[43] to account for the interband optical absorption of a-Si:H specimens in different annealing states and at different temperatures. These authors noted a linear correlation between the band gap and the Urbach parameter. He suggested that both parameters reflected a single underlying disorder — essentially the "sum" of static, frozen-in disorder, and dynamic thermal broadening. This is essentially the same basic idea we are considering, except that the roles of the valence-band tail and the conduction-band tail are interchanged.

ACKNOWLEDGMENTS

The authors thank Phillip John for computer programming, Christoph Nebel for providing his Ph.D. thesis and discussion of this paper, and Christophe Longeaud for comments and pointing out errors in the original manuscript. This research was supported by National Renewable Energy Laboratory Subcontracts Nos. XG-1-10063-7 and ZM-1-19033-2.

APPENDIX: TRANSIT TIME BASED ON HALF-CHARGE METHOD

In the dispersive transport, assuming carriers' displacement less than the sample thickness, carriers initially generated at one side of the sample drift into specimen and eventually will be deep trapped inside. Deep-trapping time characterizes this event, which is independent of the sample thickness and the electric field, and is intrinsic to the specimen. As the sample thickness decreases or the electric field increases, at certain point carriers' displacement is close to the sample thickness and some of carriers have a chance to make across. With the increase of the electric field, more carriers arrive at the other side. In this case, the transit time t_T can been measurable, which is dependent of the sample thickness and the electric field. The transit time records the mean position of a carrier distribution has reached the other side. Experimentally, the transient photocurrents do have two noticeable domains, so called the pre-transient ($t \leq t_T$) and the post-transient ($t \geq t_T$). The transit time has been used as the characteristic time to separate these two.

The multiple-trapping model predicts the power-law decay of current with time before and after the transit time t_T.[10] It obeys the following formula:

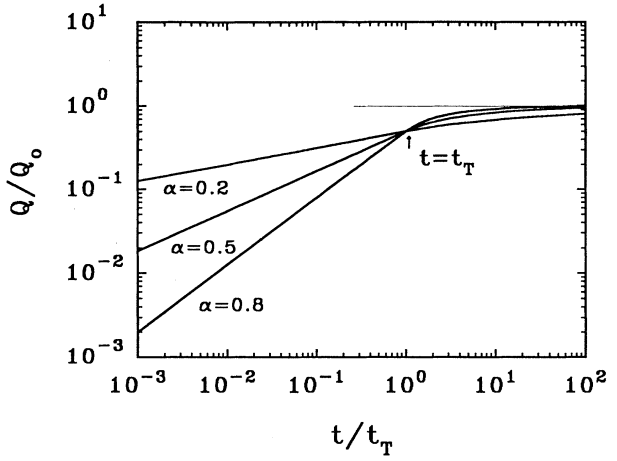

FIG. 19. Calculation of normalized transient photocharge $Q(t)$ as a function of the normalized time at three different values of dispersive parameter α. It shows that at transit time t_T the photocharge has reached half of the total charge Q_0.

$$i(t) \propto \begin{cases} t^{-(1-\alpha)} & (t \leq t_T) \\ t^{-(1+\alpha)} & (t \geq t_T), \end{cases} \tag{A1}$$

where α is a parameter ($0 \leq \alpha \leq 1$).

Now let us look at the charge transients instead of the current before and after transit time. We integrate currents and modify charge $Q(t)$ and time t in terms of total charge Q_0 and transit time t_T, and notice the charges' continuity at the transit time, then the normalized charge has the following form:

$$\eta(x) = \begin{cases} \frac{1}{2}x^{\alpha} & (x \leq 1) \\ \frac{1}{2}(1 - x^{-\alpha}) + \frac{1}{2} & (x \geq 1), \end{cases} \tag{A2}$$

where $\eta = Q/Q_0$ and $x = t/t_T$.

In Fig. 19 we have graphed the normalized charge as a function of normalized time at three different dispersive parameters α based on above equation. It has shown two important features. First, three curves focus at $t = t_T$ (transit time). It implies that at the transit time the value of the charge is independent of dispersive parameter. Second, at $t = t_T$, $Q(t_T) = Q_0/2$. It means at the transit time the terminal has collected half of the total charge (half-charge method), regardless of the values of dispersive parameter. This definition of transit time has a clear physical picture and is based on the fact that, prior to the onset carrier transit, the photocharge $Q(t)$ is proportional to the distance moved by the mean position of the photocarrier distribution. Equation (3) shows this relationship. Alternatively, it is equivalent to define the transit time as the one that carriers' displacement L has reached to half of the sample thickness d, namely, $L = d/2$. Transit time can be solved graphically.

*Present address: Center for Photoinduced Charge Transfer, 206 Gavett Hall, University of Rochester, Rochester, NY 14627-0166.

[1]G. Pfister and H. Scher, Adv. Phys. **27**, 727 (1978).
[2]H. Scher, M. F. Shlesinger, and J. T. Bendler, Phys. Today **44** (1), 26 (1991).
[3]F. W. Schmidlin, Phys. Rev. B **16**, 2362 (1977).
[4]J. Noolandi, Phys. Rev. B **16**, 4466 (1977).
[5]T. Tiedje and A. Rose, Solid State Commun. **37**, 49 (1980).
[6]J. Orenstein, M. Kastner, and V. Vaninov, Philos. Mag. B **46**, 23 (1982).
[7]T. Tiedje, J. M. Cebulka, D. L. Morel, and B. Abeles, Phys. Rev. Lett. **46**, 1425 (1981).
[8]J. M. Hvam and M. H. Brodsky, Phys. Rev. Lett. **46**, 371 (1981).
[9]J. Shirafuji, H. Matsui, Y. Inuishi, and Y. Hamakawa, Jpn. J. Appl. Phys. **22**, 775 (1983).
[10]T. Tiedje, in *Hydrogenated Amorphous Silicon II*, edited by J. D. Joannopoulos and G. Lucovsky (Springer-Verlag, New York, 1984), pp. 261–300.
[11]J. M. Marshall, R. A. Street, and M. L. Thompson, Philos. Mag. B **54**, 51 (1986).
[12]M. Stutzmann, R. A. Street, C. C. Tsai, J. B. Boyce, and S. E. Ready, J. Appl. Phys. **66**, 569 (1989).
[13]J. L. Garcia-Colevatti, Ph.D. thesis, University of Delaware, 1985.
[14]F. Karg, W. Krühler, and M. Möller, J. Appl. Phys. **60**, 6 (1986).
[15]S. Oda, S. Takgi, and I. Shimizu, Jpn. J. Appl. Phys. **25**, 49 (1986).
[16]C. E. Nebel, H. C. Weller, and G. H. Bauer, in *Amorphous Silicon Technology*, edited by A. Madan, M. J. Thompson, P. C. Tayler, P. G. LeComber, and Y. Yamakawa, MRS Symposia Proceedings No. 118 (Materials Research Society, Pittsburgh, 1988), p. 507.
[17]G. H. Bauer, C. E. Nebel, M. B. Schubert, and G. Schumm, in *Amorphous Silicon Technology—1989*, edited by A. Madan, M. J. Thompson, P. C. Tayler, Y. Yamakawa, and P. G. LeComber, MRS Symposia Proceedings No. 149 (Materials Research Society, Pittsburgh, 1989), p. 485.
[18]C. Longeaud and R. Vanderhaghen, Philos. Mag. B **61**, 277 (1990).
[19]C. E. Nebel, Ph.D. thesis, Universität Stuttgart, 1990.
[20]E. Z. Liu, D. Pang, W. Paul, and J. H. Chen, in *Amorphous Silicon Technology—1992*, edited by M. J. Thompson, Y. Yamakawa, P. G. LeComber, A. Madan, and E. A. Schiff, MRS Symposia Proceedings No. 258 (Materials Research Society, Pittsburgh, 1992), p. 529.
[21]S. Aljishi, J. Shu, and L. Ley, in *Amorphous Silicon Technology—1989* (Ref. 17), p. 125.
[22]S. Guha, J. S. Payson, S. C. Agarwal, and S. R. Ovshinsky, J. Non-Cryst. Solids **97&98**, 1455 (1987).
[23]R. Vanderhaghen and C. Longeaud, J. Non-Cryst. Solids **114**, 540 (1989).
[24]C. E. Nebel and G. H. Bauer, Philos. Mag. B **59**, 463 (1989).
[25]K. D. Mackenzie, J. R. Eggert, D. J. Leopold, Y. M. Li, S. Lin, and W. Paul, Phys. Rev. B **31**, 2198 (1985).
[26]L. Chen, J. Tauc, J.-K. Lee, and E. A. Schiff, Phys. Rev. B **43**, 11 694 (1991).
[27]N. M. Amer and W. B. Jackson, in *Hydrogenated Amorphous Silicon B*, edited by J. I. Pankove (Academic, New York, 1984), p. 83.
[28]Q. Wang, H. Antoniadis, E. A. Schiff, and S. Guha, in *Amorphous Silicon Technology—1992* (Ref. 20), pp. 881–885.
[29]H. Antoniadis and E. A. Schiff, Phys. Rev. B **43**, 13 957 (1991).
[30]H. Antoniadis and E. A. Schiff, Phys. Rev. B **44**, 3627 (1991).
[31]F. Carasco and W. E. Spear, Philos. Mag. B **47** (1983).
[32]M. Vanecek, J. Kocka, E. Sipek, and A. Triska, J. Non-Cryst. Solids **114**, 447 (1989).
[33]P. Fauchet, R. Vanderhagen, A. Mourchid, and D. Hulin, in *Amorphous Silicon Technology—1992* (Ref. 20), pp. 711–716.
[34]A. C. Hourd and W. E. Spear, Philos. Mag. B **51**, L13 (1985).
[35]R. I. Devlen, J. Tauc, and E. A. Schiff, J. Non-Cryst. Solids **114**, 567 (1989).
[36]J. M. Marshall, H. Michiel, and G. J. Adriaenssens, Philos. Mag. B **47**, 211 (1983).
[37]S. Aljishi, J. D. Cohen, S. Jin, and L. Ley, Phys. Rev. Lett. **64**, 2811 (1990).
[38]S. J. Jones, Y. Chen, D. L. Williamson, and G. D. Mooney, in *Amorphous Silicon Technology—1992* (Ref. 20), p. 229.
[39]H. Overhof and P. Thomas, *Electronic Transport in Hydrogenated Amorphous Semiconductors* (Springer-Verlag, New York, 1989).
[40]S. D. Baranovskii and M. Silver, Philos. Mag. Lett. **61**, 77 (1990).
[41]J. A. Howard and R. A. Street, Phys. Rev. B **44**, 7935 (1991).
[42]B. V. Roedern and A. Madan, Philos. Mag. B **63**, 293 (1991).
[43]G. D. Cody, T. Tiedje, B. Abeles, B. Brooks, and Y. Goldstein, Phys. Rev. Lett. **47**, 1480 (1981).
[44]D. S. Shen, J. P. Conde, S. Aljishi, Z. E. Smith, V. Chu, J. Koldzey, and S. Wagner, in *Proceedings of the 19th Photovoltaic Specialists Conference* (IEEE, New York, 1987), p. 884.
[45]K. D. Mackenzie and W. Paul, J. Non-Cryst. Solids **97&98**, 1055 (1987).
[46]Q. Wang, H. Antoniadis, and E. A. Schiff, Appl. Phys. Lett. **60**, 2791 (1992).